American Mineralogist, Volume 100, pages 1762–1777, 2015

SPECIAL COLLECTION: PERSPECTIVES ON ORIGINS AND EVOLUTION OF CRUSTAL MAGMAS

Field and model constraints on silicic melt segregation by compaction/hindered settling: The role of water and its effect on latent heat release†

Cin-Ty A. Lee[1,*], Douglas M. Morton[2], Michael J. Farner[1] and Pranabendu Moitra[1]

[1]Department of Earth Science, MS-126, Rice University, 6100 Main Street, Houston, Texas 77005, U.S.A.
[2]Department of Earth Sciences and United States Geological Survey, 900 University Avenue, University of California, Riverside, California 92521, U.S.A.

Abstract

To investigate how large volumes of silicic melts segregate to form granitic plutons, we conducted a case study of a zoned pluton, in which SiO_2 increases from intermediate (69 wt%) to highly silicic compositions (74 wt%) toward the contact with metasedimentary wallrock in the outer 25 m of the pluton. All other major, minor, and trace elements vary systematically with SiO_2 and indicate that outward increasing SiO_2 is due to a decrease in mafic elements and minerals. Whole-rock oxygen isotopes and elemental variation diagrams do not support mixing with wallrock as an explanation for the Si-rich boundary layer. Instead, mafic enclaves, which are common in the pluton, also decrease in abundance in the outer 25 m of the pluton, suggesting a mechanical origin for the Si-rich boundary layer. The coupling of mechanical and geochemical boundary layers, combined with geochemical modeling, indicate that the silica-rich, enclave-poor boundary layer formed by hindered settling or compaction of a crystal-rich (crystal fractions >60%) magmatic mush. Segregation of melts at high crystal fraction is known to be a slow process. However, petrography and Zr-based thermometry indicate that the residual Si-rich liquids were water-saturated. Water decreases melt viscosity, which helps expulsion, but equally importantly, water also delays much of the latent heat release to late in the thermal and crystallization history of a cooling magma. We show that the higher the water content, the longer the time interval over which a magma chamber resides at the stage when water-saturated, high-silica liquids form, allowing sufficient time for exfiltration of silicic liquids before the magma body freezes.

Keywords: Granite, rhyolite, batholith, pluton, cumulate, compaction, settling, xenolith

Introduction

The ubiquity of highly silicic igneous rocks, such as granites, at Earth's surface makes our planet unique in the Solar System (Campbell and Taylor 1983; Taylor and McLennan 1985).

Of interest are how magmas with SiO_2 contents greater than 70 wt% are formed. Volumetrically, most magmatism on Earth occurs by melting of the ultramafic mantle, but this process produces basalts. Making silicic magmas from more mafic parents requires a multi-stage differentiation process. For example, extreme fractionation (>95% crystal separation) is needed to make granites (Lee and Morton 2015). Numerous hypotheses have been suggested: crystal settling from more primitive parental magmas, partial melting (anatexis) of pre-existing crust or sediments, compaction-driven crystal segregation, Soret diffusion, zone refining, thermal migration, liquid immiscibility, or assimilation of Si-rich metasediments (Atherton 1993; Bachl et al. 2001; Bachmann and Bergantz 2004, 2008; Bacon and Druitt 1988; Baker and McBirney 1985; Beard and Lofgren 1991; Bowen 1928; Brown 1994; Brown et al. 1995; Castro 2013; Castro et al. 2010; Chappell 1999; Clemens and Stevens 2012; Glazner et al. 2008; Hildreth 1979; Hildreth and Wilson 2007; Jagoutz and Schmidt 2012; Lipman 2007; Lundstrom 2009; McBirney 1980; Noyes et al. 1983; Philpotts 1976; Ratajeski et al. 2005; Roedder 1951; Tuttle and Bowen 1958; Van Tongeren and Mathez 2012). To contribute to this topic, we examine a well-exposed tonalitic pluton in which compositions grade from intermediate to high silica contents at the pluton margin. We combine geochemical, petrologic, and field observations to determine the mechanism by which the Si-rich boundary layer formed. In this case study, the observations are best explained by compaction-driven segregation of silicic liquids. We combine our observations with thermodynamic models to define the compositional and physical conditions of the magmatic system over which compaction operated.

Study area: Domenigoni Valley pluton, California

The study site is located within the Cretaceous 120 Ma Domenigoni Valley pluton in the northern Peninsular Ranges Batholith in southern California (Morton et al. 2014) (Fig. 1). The pluton comprises a minimum area of ~160 km^2 and intruded into a Jurassic meta-sedimentary unit composed of meta-greywacke, interlayered calcareous quartzite and phyllite-schist (Morton et al. 2014) (Figs. 1 and 2). The pluton consists of isotropic, medium-grained biotite-hornblende tonalite with accessory zircon, titanite

* E-mail: ctlee@rice.edu

† Special collection papers can be found on GSW at http://ammin.geoscienceworld.org/site/misc/specialissuelist.xhtml.

0003-004X/15/0809–1762$05.00/DOI: http://dx.doi.org/10.2138/am-2015-5121

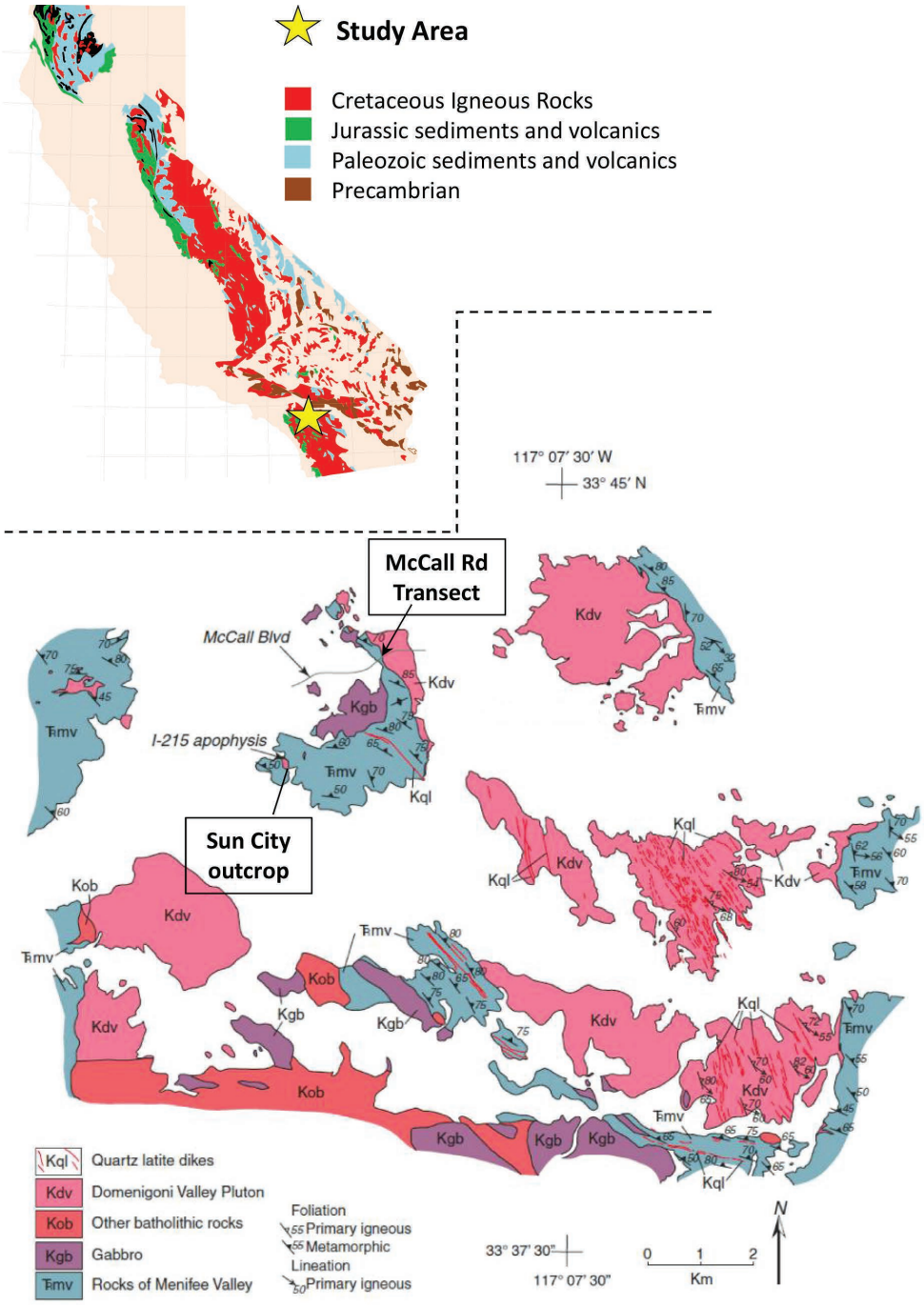

FIGURE 1. Location map of the Domenigoni Valley Pluton. Study area of the McCall Blvd. transect in Figure 2 is labeled. Sun City outcrop where metasedimentary xenoliths have been previously studied (Liao et al. 2013) is also shown. (Color online.)

(e.g., sphene), apatite, and magnetite-ilmenite. The pluton itself lies within the western zone of the Peninsular Ranges batholith, interpreted to represent juvenile magmas intruded into a Jurassic island arc basement accreted onto the margin of North America (Busby 2004; Gastil et al. 1988; Gastil 1975; Kistler et al. 2003; Lee et al. 2007; Morton et al. 2014; Todd et al. 1988). Metamorphic grade of the meta-sediments range from greenschist to amphibolite. Clearly exposed contacts between the metamorphic rocks and the pluton are discordant, as exemplified by truncated metamorphic fabrics (Fig. 2). The presence of porphyritic apophyses emanating into the metamorphic wallrock suggests that the exposed area was structurally near the top of the magma chamber (Morton et al. 2014). Mafic enclaves and metasedimentary xenoliths are common throughout the pluton (Liao et al. 2013; Morton et al. 2014).

We investigated a well-exposed horizontal transect extending 70 m from the wallrock into the pluton (Fig. 2). This transect

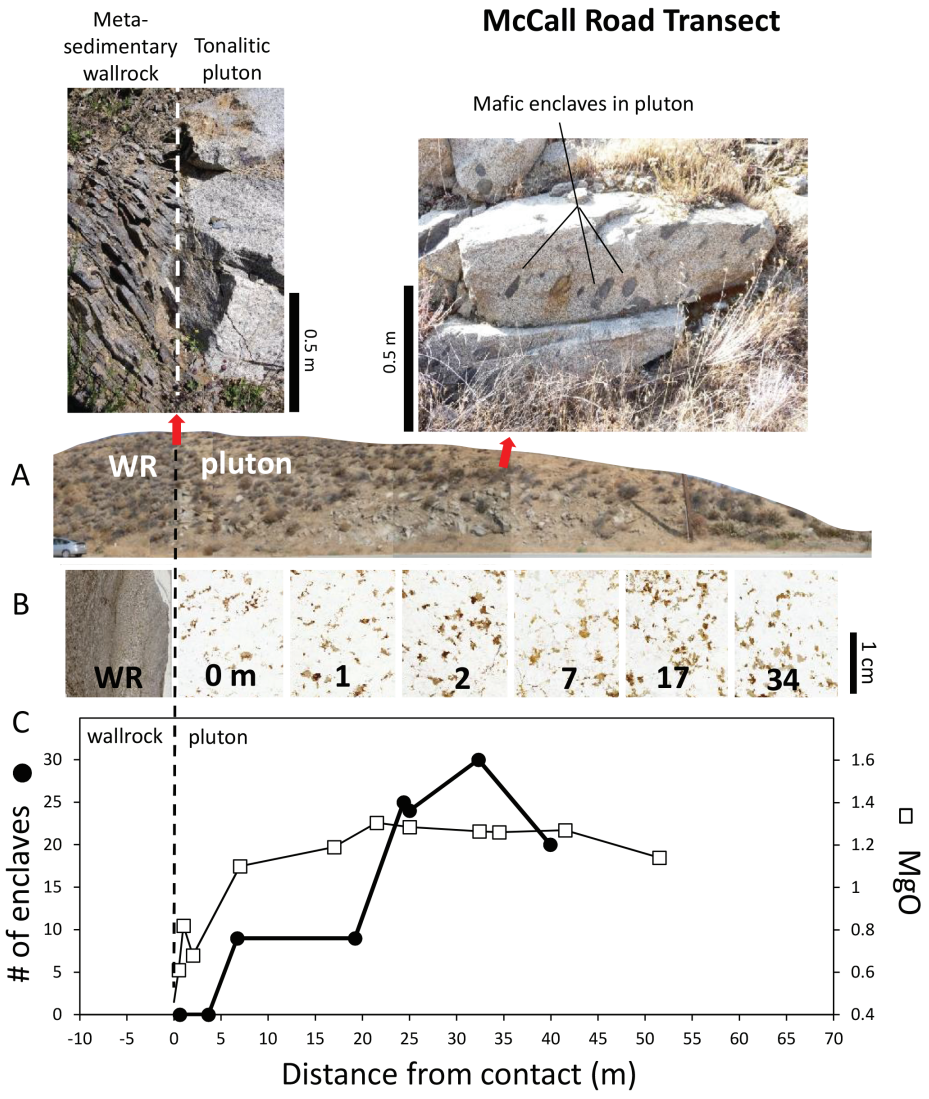

Figure 2. Photograph of the roadcut along McCall Blvd. in Menifee (formerly Sun City), California (33°43′13.32″ N; 117°09′46.94″ W) with Toyota Prius for scale at far left. Wallrock (WR) contact with pluton is denoted by vertical dashed line. Insets above **a** show close up views of the contact and the pluton along with examples of mafic enclaves. (**b**) Photomicrograph thin sections in plane light sampled at different distances from the contact (numbers represent meters). Brown minerals are hornblende and biotite; clear minerals are quartz and feldspars. (**c**) Plot of the number of enclaves per 2 × 2 m square (left axis) and bulk rock MgO content of the pluton (excluding enclaves) are plotted with distance from the contact. (Color online.)

is exposed along the north side of McCall Boulevard (Blvd. hereafter) at 33.720391° N and 117.163093° W in the town of Menifee, California (Fig. 1) and is the same transect studied by Turi and Taylor (1971) for oxygen isotopes. Mafic enclaves of igneous origin, but no metasedimentary xenoliths, are found in this transect. We refer in this study to another section of the pluton where metasedimentary xenoliths (pelitic, quartzo-feldspathic, and calc-silicate protoliths) are present and in varying states of thermal and chemical equilibration with the pluton (Liao et al. 2013) (Fig. 3a). This outcrop, which we refer to as the "Sun City" locality, is located on the east side of Highway 215 at 33.702514° N and 117.182052° W although it is no longer safe to access (Fig. 1).

Method

We collected samples along a surveyed transect across the roadcut, taking care to avoid contamination by mafic enclaves. Enclave abundance was estimated visually in 2 × 2 m squares along the transect. Thin sections were made for selected samples along the transect. The proportions of biotite and hornblende were quantified from scanned thin section images using ImageJ software. Whole-rock analyses were completed at the USGS by fusion of powders followed by solution ICP-AES. Mineral chemistries were determined by laser ablation ICP-MS at Rice University (Lee et al. 2009). Data are available in the supplementary tables (Appendix Tables 1–6[1]).

[1] Deposit item AM-15-85121, Appendix Tables 1–6. Deposit items are free to all readers and found on the MSA web site, via the specific issue's Table of Contents (go to http://www.minsocam.org/MSA/AmMin/TOC/).

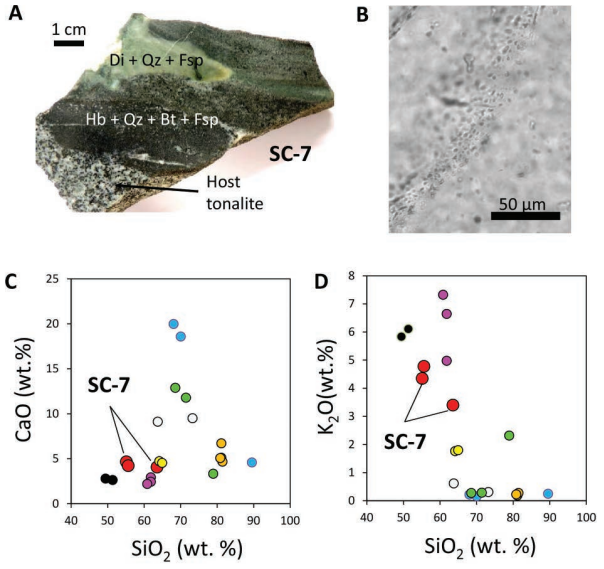

Figure 3. (**a**) Zoned calc-silicate metasedimentary xenolith [sample SC-7 from (Liao et al. 2013)] from Sun City location in the Domenigoni Valley pluton. Di = diopside, Qz = quartz, Fsp = feldspar, Hb = hornblende. (**b**) Fluid inclusions in healed fractures in quartz within the tonalite pluton at McCall Blvd. (**c** and **d**) Compositions of metasedimentary xenoliths from Sun City location (Liao et al. 2013). Samples from the same xenolith but different sections of the xenolith share identical colored symbols. Sample SC-7 from **a** is shown. Limited intra-xenolith compositional variation is seen, suggesting isochemical transformation with the exception of the ingress of water to convert diopside to hornblende. (Color online.)

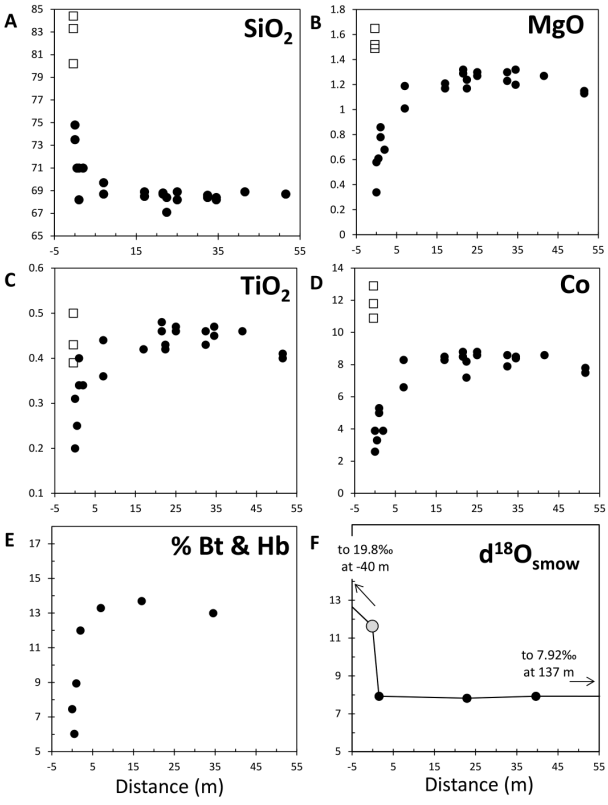

Figure 4. Compositional transects across the contact and into the pluton at McCall Blvd. Plutonic rocks are represented by solid black circles. Wallrock represented by open squares. (**a**–**d**) SiO_2, MgO, TiO_2, and Co vs. distance; oxides are in weight percent, but Co is in parts per million by weight. (**e**) Modal percent of biotite+hornblende in the pluton as estimated by image analysis of thin sections. (**f**) Whole-rock oxygen isotopic (‰ deviation from SMOW) composition from Turi and Taylor (1971).

Results

Pluton

Petrography and whole-rock geochemistry. The pluton is tonalitic and dominated by biotite, hornblende, plagioclase, and quartz. Accessory minerals include apatite, zircon, titanite, and Fe-Ti oxides. Fluid inclusions are abundant in healed fractures of quartz and plagioclase (Fig. 3b), which suggest that the pluton had reached saturation in a free, likely water-rich, fluid phase. Whole-rock major and trace elements of the pluton co-vary in the outer 25 m of the pluton, becoming more silicic and less mafic toward the wallrock contact (Figs. 2c and 4, Appendix Table 1[1]): SiO_2 increases from ~68 wt% in the pluton interior (>25 m) to 75 wt% at the contact while Mg, Fe, Ca, and Co decrease (concentrations reported on a volatile-free basis) (Fig. 4). Mafic mineral abundances (hornblende + biotite), as determined by image analysis of scanned thin sections, decrease from 25 m in the pluton toward the wallrock contact (Fig. 4e). The compositional zonation across the 25 m outer margin yields correlated arrays in element-element variation diagrams (Figs. 5a and 5b). These correlated arrays can be explained by mixing/unmixing of a hornblende-biotite-plagioclase component (Figs. 5a and 5b). They do not show any hint of mixing with metasedimentary wallrock.

Some whole-rock quantities do not vary across this boundary layer. Previous work (Turi and Taylor 1971) has shown that whole-rock $\delta_{SMOW}{}^{18}O$ remains constant at ~8‰ across this boundary (Fig. 4f), indicating no immediate effect of reaction with or assimilation of the metasedimentary wallrock (19.8‰). Whole-rock Zr concentrations are also relatively constant [Appendix Table 1[1]; 113 ppm ±30 ppm (1 σ)]. Zr whole-rock concentrations suggest an apparent temperature of ~750 °C (Fig. 6a, Appendix Table 1[1]), assuming the liquid was saturated in zircon (Boehnke et al. 2013; Watson and Harrison 1983), which is reasonable given that Zr contents of the tonalites as a whole are lower than more intermediate rocks in the Peninsular Ranges Batholith (Lee and Bachmann 2015). We note that if zircon-saturated magmas contain inherited zircon or excess crystal cargo ("cumulate" zircon), the estimated zircon saturation temperatures are maximum bounds, and if they were initially under-saturated, the estimated temperatures are minimum bounds (Miller et al. 2003).

Mineral chemistries. We also analyzed the compositions of plagioclase, biotite, and quartz in the pluton across the transect (Appendix Tables 4–6[1]). Plagioclase anorthite varies between 25–35 mol% in a given thin section, but not across the transect (Fig. 6b). In contrast, biotite compositions vary across the 25 m boundary layer: Mg and Co contents of biotite decrease toward the contact, consistent with increasing felsic nature of the bulk

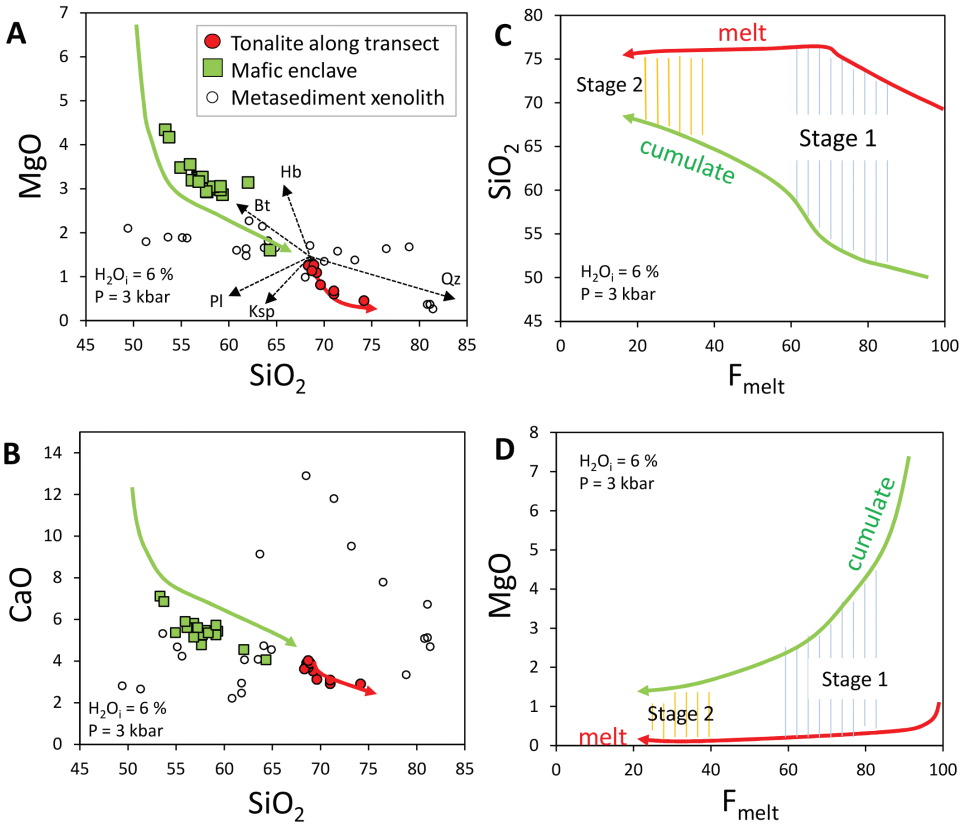

Figure 5. (**a** and **b**) MgO and CaO vs. SiO_2 (wt% on anhydrous basis) of the pluton (yellow circles) and mafic enclaves (green squares) from the McCall Blvd. transect. Wallrocks and metasedimentary xenoliths from McCall Blvd. and Sun City locations, respectively, are shown as small open circles. Green and red lines represent isobaric (3 kbar) closed system rhyolite-MELTS models for the liquid (red) and crystal (green) lines of descent of a parental tonalite composition at 55 m from the contact and an assumed system water content of 6 wt%. Arrows indicate direction of cooling and decreasing residual melt fraction. In **a**, dashed arrowed lines point toward mineral end-members. (**c** and **d**) SiO_2 and MgO (wt% on anhydrous basis) of model residual liquid formed during crystallization of the parental tonalite plotted as a function of residual melt fraction F. Color of lines correspond to the same as in **a** and **b**. Compositions of melt and cumulate in equilibrium are shown with tie lines. Stage 1 cumulates could be represented by the mafic enclaves in the McCall Blvd. transect and can be seen here to be in equilibrium with the parental tonalite, suggesting that the mafic enclaves may represent cognate cumulate xenoliths entrained as cargo in the parental tonalite when it rose and became emplaced into the upper crust. There is a distinct absence of enclaves having compositions between ~62–70 wt% SiO_2 despite model results that predict such lithlogies should have formed. Final extraction of Si-rich melts (75 wt%) leaves behind a "cumulate" with approximately the same composition of the parental tonalite. We refer to these cumulates as stage 2 cumulates. Crystallization models are done using rhyolite-MELTS (Gualda et al. 2012). (Color online.)

rock toward the contact (Fig. 6c). Ti and P contents of quartz show no variation across the transect (Fig. 6d). The Ti contents in the quartz define temperatures of ~580–680 °C, assuming rutile saturation (Wark and Watson 2006). Assuming a lower bound of 0.6 for TiO_2 activity gives Ti-in-quartz temperatures of 680–780 °C. We note that the ~100 °C variation in temperatures within a given thin section likely reflects sluggish diffusion of Ti rather than analytical uncertainties. Phosphorus, whose concentration in quartz should be buffered by the presence of apatite, is also a sluggish diffusing element, correlating with Ti in quartz (Fig. 6d). The low Ti-in-quartz temperatures are consistent with the Zr saturation temperatures.

Enclaves and xenoliths

Mafic enclaves from the McCall Blvd. transect. Mafic enclaves, ranging in size from 5–20 cm, are common in the Domenigoni Valley pluton. These mafic enclaves along the McCall Blvd. transect are amphibole- and biotite-rich, consistent with their more mafic compositions compared to the tonalite (Appendix Table 2[1]). They are distinctly different in composition from the metasedimentary xenoliths, described below. In elemental variation diagrams, the McCall Blvd. mafic enclaves define arrays that are complementary to the arrays defined by the tonalites along the transect, suggesting that they may be cumulates associated with the formation of some of the tonalites (Figs. 5a and 5b). The number density of enclaves across the transect decreases from 5–7.5/m^2 beyond 25 m to none at the contact (Fig. 2c; Appendix Table 3[1]). Variation in the spatial abundance of enclaves suggests redistribution by advective or mechanical processes. The coincidence of the spatial variation in enclave abundance and tonalite composition requires that mechanical and chemical processes responsible for differentiating the magma body are coupled.

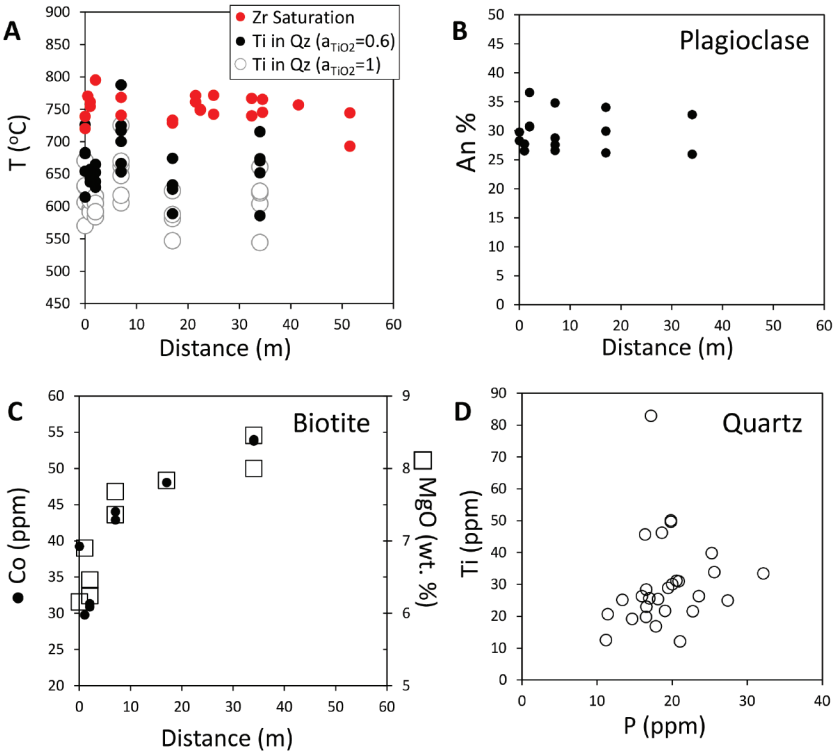

Figure 6. (**a**) Various estimates of magmatic temperatures from McCall Blvd. transect plotted vs. distance from contact. Red symbols are apparent Zr saturation temperature as inferred from whole-rock Zr contents and Zr solubility models (Watson and Harrison 1983). Circles represent Ti-in-quartz temperatures assuming TiO_2 activities of 1 (open symbols) and 0.6 (black symbols). (**b**) Plutonic plagioclase anorthite content in pluton vs. distance. (**c**) Plutonic biotite Co (ppm; black circles) and MgO (wt%; open squares) concentrations vs. distance. (**d**) Ti and P elemental concentrations (parts per million) in plutonic quartz. (Color online.)

Metasedimentary xenoliths from the Sun City outcrop. Xenoliths with metasedimentary wallrock protoliths are also present (Figs. 3a, 3c, and 3d). These are absent from the McCall Blvd. locality but common elsewhere, such as at the Sun City outcrop. In a previous study (Liao et al. 2013; Morton et al. 2014), we showed that the xenolith protoliths are pelites, quartzites, and calc-silicates, which underwent varying extents of thermal metamorphism and reactive equilibration with the host tonalitic magma. We discuss these xenoliths briefly for completeness because they are relevant to interpreting the magmatic history. The entire sequence of metamorphic reactions is observed, beginning with calcite- and dolomite-bearing sandstones in the wallrock, followed by thermal metamorphism and decarbonation to wollastonite and diopside after entrainment into the pluton, and ending with transformation of diopside to hornblende with an increase in water activity (and decrease in CO_2 activity). This sequence of reaction is expressed as core to rim variations in mineralogy even in individual xenoliths (Liao et al. 2013). For example, Figure 3a shows a sample with a diopside-rich core surrounded by a hornblende-rich mantle. Notably, the bulk compositions of different sections of mineralogically zoned xenoliths are relatively constant except for water (Figs. 3c and 3d). This suggests that, initially, some of these xenoliths were thermally metamorphosed in a closed system except for the rapid diffusion of water into the xenolith. We consider this as indirect evidence that free water permeated the xenoliths and transformed the calc-silicate xenoliths into amphibolites.

Discussion

The origin of a Si-rich outer boundary layer is perplexing. Cooling of a magma body should initiate from the margins, causing crystallization fronts to migrate inward and generate margins composed of mafic "cumulates" and plutonic cores of more silicic residual magmas; such zonation is commonly seen in mafic magma bodies (McBirney 1995; Pitcher 1997). The outward increase in Si in this study thus seems atypical (Pitcher 1997), but this reverse zonation may not be that unusual in felsic systems. Felsic plutons with silicic roofs or margins have been reported (e.g., Hutchinson 1956; Fridrich and Mahood 1984; Allen 1992). The eruption sequence of ignimbrite deposits often suggest that the top of felsic magma chambers are more silicic (Hildreth and Wilson 2007). Outer silicic margins are also seen in some nested plutons (Allen 1992; Coleman et al. 2004).

How do these Si-rich boundary layers form?

Some scenarios can be ruled out for this particular case study. Local mixing with metasedimentary wallrocks is not evident in any elemental variation diagrams or in the constant oxygen isotopes (Figs. 4 and 5) (but mixing earlier in the magmatic history likely occurred). Soret and thermo-chemical diffusion (Lund-

strom 2009) are inconsistent with the strong spatial coupling between all the elements and the xenolith abundances because elements with different diffusivities should develop boundary layers with different characteristic length scales.

Coupled chemical and mechanical boundary layers instead require physical segregation of liquids from mineral grains *and* the mafic enclaves. Segregation of mafic minerals, like amphibole and plagioclase can explain the linear arrays in elemental variation diagrams, such as the negative correlation of MgO and CaO with SiO_2. Possible segregation scenarios include compaction-driven expulsion of residual liquids (Bachmann and Bergantz 2004; Dufek and Bachmann 2010; McKenzie 1984, 1987), hindered settling of crystals (Bachmann and Bergantz 2004), and shear-induced self-diffusion of crystal grains (Barker 2000; Leighton and Acrivos 1987; Ross 1986). Shear-induced flow segregation drives migration of crystal grains away from a high strain boundary layer if there are gradients in crystallinity or effective viscosity perpendicular to large-scale streamlines (Leighton and Acrivos 1987). If plutons are colder on their margins, higher viscosity and crystallinity on the margins would be expected, so particles might be expected to migrate toward the warmer lower viscosity interior of the magma body owing to asymmetrical inter-grain interactions across the shear boundary layer. However, the migration efficiency (which follows a "diffusive" law) of particles undergoing shear-driven migration should scale with the square of the particle radius, so large particles should migrate farther than small particles (Leighton and Acrivos 1987). This is not supported by the observation that the abundances of mafic minerals and the much larger mafic enclaves vary over the same length scale. Free gravitational settling of crystals also cannot explain the observations because settling velocities similarly scale with the radius squared, causing the transport distances of large particles (enclaves) to differ from mineral grains, which we do not see.

Compaction or hindered settling may be the most plausible mechanism by which coupled mechanical and chemical boundary layers form. Hindered settling occurs at intermediate crystal fractions (20–40%), wherein the separation distance between grains is small enough that differential settling is hindered by viscous interaction between the grains. Compaction occurs by deformation of the crystal mush solid framework and can operate at higher crystal fractions (>40%). In both scenarios, crystal-liquid segregation is driven by differential buoyancy between crystals and liquids, or in the case of compaction, by internal and external stresses as well. The low temperatures (~750 °C) recorded by whole-rock Zr contents and Ti-in-quartz temperatures are well below the liquidus of the tonalitic host, consistent with the granitic boundary layer deriving from a late stage, crystal-rich magma. Depending on the amount of water in the system, crystal fractions at these temperatures can vary from 20 to more than 80%, well within the regime for hindered settling or compaction. Our study provides outcrop confirmation for a compaction origin for the generation of silicic magma bodies (Bachmann and Bergantz 2004).

Petrogenesis of the silica-rich boundary layer

To explore the crystal-liquid segregation scenario further, we used rhyolite MELTS (Gualda et al. 2012) to model crystal-melt equilibria of the host pluton (MR11c at 51.5 m away from the contact; 60–70 wt% SiO_2) during cooling and crystallization at 3 kbar, corresponding to the average Al-in-hornblende pressures for plutonic rocks in the region (Ague and Brimhall 1988a; Ague and Brimhall 1988b). We assume closed system equilibration (batch), that is, liquids and crystallized products are not removed from the system and are always assumed to be in thermal and chemical equilibrium. An oxygen fugacity equivalent to the fayalite-magnetite-quartz buffer was assumed. We modeled melting/crystallization of bulk systems with water contents varying from 0 to 6 wt% H_2O (Fig. 7).

We compare the modeled geochemical evolution of a crystallizing hydrous tonalite system (6 wt% H_2O) to the compositions of the mafic enclaves and the tonalite compositions along the McCall Blvd. transect in Figure 5 (a more detailed discussion on the effects of variable water content are in the next section). Mafic enclaves with SiO_2 between 52–60 wt% SiO_2 are consistent with being cumulates in equilibrium with the parental tonalitic liquid (69–70 wt% SiO_2) at model melt fractions of 60–100%, although it is equally possible that the mafic enclaves represent quenched magmas. The most silicic melts (75 wt% SiO_2), on the outermost margin of the pluton, require >40% crystallization of the parental tonalite ($F < 60\%$), but there are few cumulate xenoliths having compositions in equilibrium with low F (<60%) melts, except for the host tonalite itself. Enclaves with compositions between 60–70 wt% SiO_2 are absent despite our models predicting their existence if melts were extracted continuously during the crystallization process (Figs. 5c and 5d). However, at model melt fractions F < 20%, hypothetical cumulate compositions in equilibrium with a melt having 75 wt% SiO_2 are nearly indistinguishable from the parental tonalite in terms of major elements (Figs. 5c and 5d). Thus, the "cumulate" in equilibrium with the high silica boundary layer may be represented by the host tonalite itself [see also Gelman et al. (2014) and Lee and Bachmann (2015)].

We suggest that the host magma and mafic enclaves were formed together by crystal fractionation of a more primitive magma, presumably at greater depths. The magma then rose into the upper crust, carrying mafic enclaves. After stalling in the upper crust, the magma body cooled and crystallized, generating a crystal-rich mush with a silica-rich residual melt filling the porosity. This Si-rich melt segregated to generate the Si-rich boundary layer, leaving behind a felsic cumulate (likely with intercumulus melt), whose composition is nearly indistinguishable from the parental tonalite itself due to the low melt fractions extracted (Gelman et al. 2014; Lee and Morton 2015).

Conditions of silicic melt generation and the role of water: Observations and thermodynamic models

Insight into the role of water during crystallization of the host tonalite magma can be had from thermodynamic models of melting/crystallization of the host tonalite (MR11c) using rhyolite MELTS (Gualda et al. 2012). Four key effects are noted here:

(1) Water changes the temperature interval over which melting occurs (Figs. 7a and 7b). Liquidus temperatures decrease with increasing dissolved water content (Boettcher and Wyllie 1968; Castro 2013). As the magmatic system (crystals + melt) cools and crystallizes, the melt fraction decreases and the water content

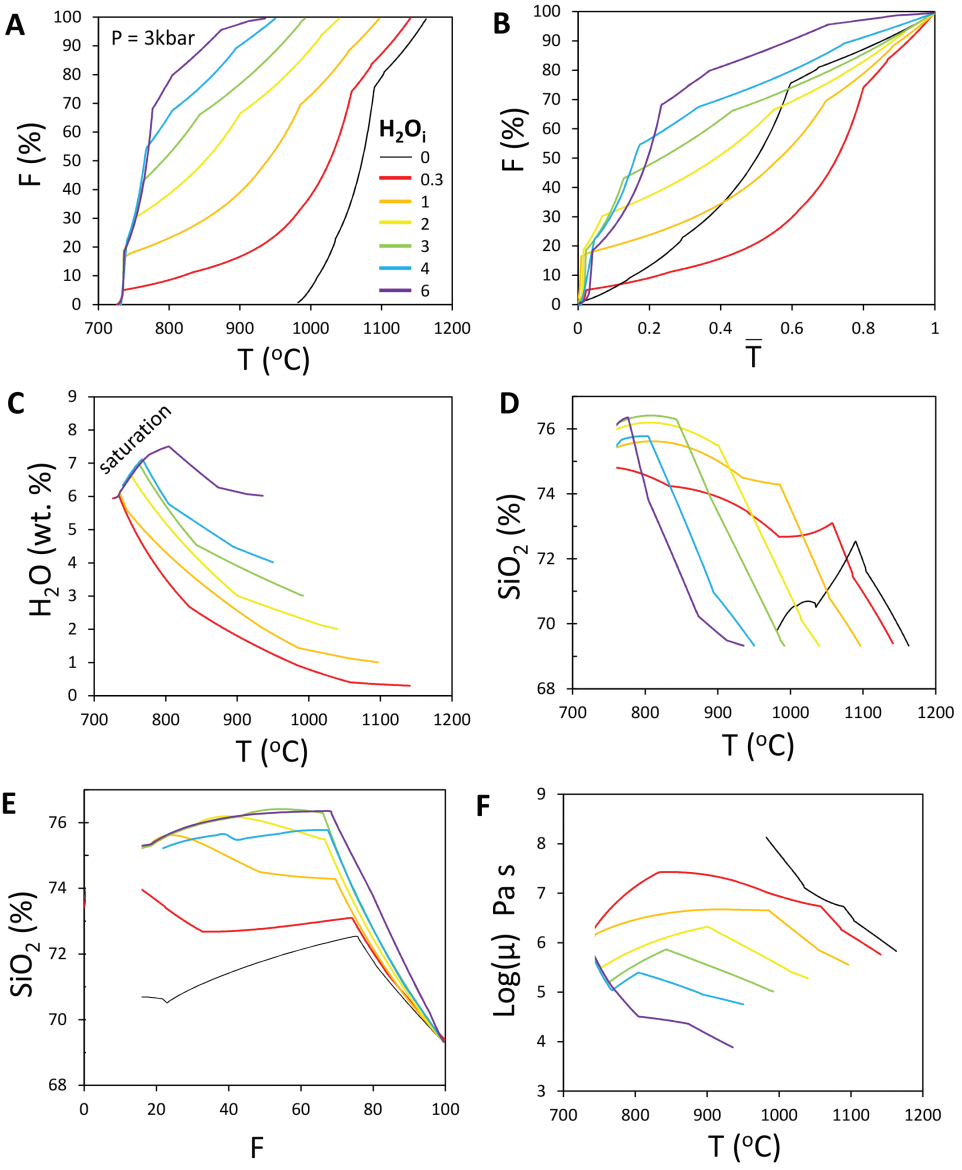

FIGURE 7. Thermodynamic models of liquid lines of descent from a parental tonalite having a composition equal to the tonalite at ~50 m inward of the pluton margin. (**a**) Melt fraction (*F*) as a function of temperature for different bulk system water contents (H_2O_i) based on rhyolite MELTS modeling (Gualda et al. 2012; Pamukcu et al. 2013). Lines are colored for different bulk water contents. (**b**) Same as in **a** but temperature has been re-normalized to the temperature difference between the solidus and the liquidus. (**c**) H_2O wt% in the residual melt as a function of temperature. H_2O contents rise with cooling because H_2O behaves as an incompatible element. (**d**) SiO_2 (wt%) in the residual melt vs. temperature. (**e**) SiO_2 (wt% on anhydrous basis) in the residual melt vs. melt fraction F. H_2O concentrations are bounded by the saturation curve. (**f**) Viscosity of the melt (Pa s) plotted vs. temperature of the system. Note that this is *not* a plot showing how temperature influences melt viscosity. These curves are controlled by a combination of H_2O, temperature, and melt composition, all of which change during crystallization. SiO_2 contents for melt fractions below ~15% are not reported. (Color online.)

in the melt increases because water is preferentially partitioned into the melt fraction, which decreases with progressive cooling (Fig. 7c). Water continues to rise until saturation, which at 3 kbar for silicic melts occurs at ~6–7 wt% H_2O (Fig. 7c). Water concentration in the residual melt scales approximately with the inverse of melt fraction $1/F$ (Jahns and Burnham 1969). In detail, the inverse relationship with F is of course modulated by the precipitation of hydrous minerals like amphibole (Jahns and Burnham 1969). But so long as the system contains reasonable amounts of water (>1%), saturation is always achieved and all magma bodies can in theory remain molten to minimum melting temperatures (~650 °C). Systems with high water saturate early (high F), generating large volumes of water-saturated melts, whereas relatively dry systems require extreme fractionation (e.g., when F approaches zero) to achieve saturation.

The above concepts can be restated in the context of melt

productivity, dF/dT, which describes how much melt F is generated per unit increase in temperature T (or conversely, how much crystallization occurs per unit decrease in temperature). In a dry system, dF/dT is relatively constant, that is, $F(T)$ is approximately linear. In a closed, water-rich system, $F(T)$ is nonlinear (Fig. 7b): melt productivity, dF/dT, is greatest when the system is near or at saturation (Pamukcu et al. 2013). Thus, in water-rich systems, high melt fractions are permissible at near-solidus temperatures, but in water-poor systems, the volume of near solidus melts is small. In part, these effects arise because the evolution of a free fluid phase results in decreased variance of the system, generating eutectic-like behavior, which promotes high melt productivity at the solidus.

(2) Water can enhance the SiO_2 (on an anhydrous basis) content of the residual melt because water facilitates the precipitation of amphibole, a low SiO_2-bearing phase (Holloway and Burnham 1972; Huang and Wyllie 1986; Kawamoto 1996), although amphibole is not explicitly modeled in the rhyolite-MELTS modeling we have done. The higher the water content (>1 wt%), the more amphibole that can precipitate, generating high-silica residual melts. Fractionation of a dry tonalite does not generate significant amounts of high-silica melts. For example, initial water contents greater than 2 wt% would generate melts with 75 wt% SiO_2 after only 20–30% crystallization (F = 70–80%), yielding large quantities of granite (Figs. 7d and 7e). These initial water contents are relatively modest given that parental basalts in arc environments often already have 4 wt% H_2O (Plank et al. 2013) and that any subsequent magmatic recharge and crystal fractionation would only increase this value (Lee et al. 2014).

(3) Dissolved water in silicate melts decreases melt viscosity by two to three orders of magnitude (Hui and Zhang 2007) (Fig. 7f). Thus, during cooling and crystallization of a magma chamber, the viscosity increase of the melt imparted by decreasing temperatures and increasing silica content is counteracted by the decrease in viscosity associated with the ever-increasing water contents of a diminishing melt fraction (this consideration of viscosity pertains only to the melt, not to the effective viscosity of a crystal+liquid mush). The compensating effect of water on viscosity is most pronounced, as expected, for water-rich systems. This decrease in melt viscosity, as we show below, increases the rate at which melts can be expelled by compaction or hindered settling.

(4) Finally, changes in the shape of $F(T)$ imparted by water will affect the rate at which latent heat is released (Fig. 7b). We will return to this property later.

Timescales of compaction and hindered settling

Segregating silicic melts from a crystal-rich magma is thought to operate too slowly for sufficient amounts of liquids to be expelled before the magma body freezes [see Jackson et al. (2003) for discussion]. We begin with the problem of segregating silicic melts from a magma with a crystal volume proportion greater than 30–40%, corresponding to a porosity of less than 60–70% (we will treat porosity here as approximately equal to the melt fraction F). At intermediate porosities, 60–70%, settling of individual crystals will initially be hindered by viscous interaction with neighboring crystals. As porosity decreases, viscous coupling with neighboring crystals increases the extent that a deformable long-range framework of crystals is formed. And with further decrease in porosity, the framework becomes largely locked, though the framework as a whole can still deform under its own weight or by external stresses. In all these cases, we assume that the crystal-rich magma does not convect because effective viscosities increase by orders of magnitude with increasing crystal volume fraction (decreasing porosity) (Dufek and Bachmann 2010; Lejeune and Richet 1995; Mader et al. 2013; Marsh 1981; Moitra and Gonnermann 2015). We thus treat melt-crystal segregation by hindered settling and compaction, following the spirit of Bachmann and Bergantz (2004).

We first estimate the rates of hindered settling at the top of a crystal-rich suspension, e.g., the magma body, using two empirical approaches. In the first (Richardson and Zaki 1954; Snabre and Pouligny 2008), the fall rate V of crystals at the top of the magma body decreases with mean crystal volume fraction χ as (Table 1):

$$V = v(1-\chi)^n \tag{1}$$

where n is ~5 for settling of ideal spheres in purely hydrodynamic interactions (e.g., no electrostatic attractions or surface tension) and v is the Stokes velocity

$$v = \frac{2\Delta\rho g R^2}{9\mu} \tag{2}$$

where g is gravitational acceleration, $\Delta\rho$ is the difference in density between solid crystals ρ_S and liquid ρ_L, R is the average crystal radius, and μ is the melt viscosity (Pa s). A second formulation, following Bachmann and Bergantz (2004), for hindered settling is given by Barnea and Mizrahi (1973),

Table 1. List of parameters and symbols

Symbol	Definition	Units
V	Hindered settling velocity	m/s
v	Stoke's settling velocity	m/s
χ	Crystal volume fraction in magma	
ϕ	Porosity	
$\Delta\rho$	Density difference between crystals and melt	kg/m^3
ρ_m	Density of magma body	kg/m^3
ρ_L	Density of silicate liquid	kg/m^3
ρ_S	Density of solids	kg/m^3
g	Gravitational acceleration	m/s^2
R	Crystal radius	m
δ_c	Compaction length scale	m
k_ϕ	Permeability	m^2
F	Melt fraction	
dF/dT	Melt productivity	°C^{-1}
μ	Viscosity of silicate liquid (melt)	Pa s
ζ	Effective bulk viscosity of crystal matrix	Pa s
η	Effective shear viscosity of crystal matrix	Pa s
w_o	Relative velocity between melt and crystals at top of crystal mush	m/s
T	Temperature	°C
T_S	Solidus temperature	°C
T_L	Liquidus temperature	°C
$\overline{T}$	Dimensionless temperature	
t	Time	s
Δt	Time increment	°C
L	Total latent heat	J/kg
c	Specific heat	J/kg°C
k	Thermal conductivity	W/m°C
κ	Thermal diffusivity (= $k/\rho c$)	m/s^2
x	Distance	m
C_o	Weight concentration of element in system	
a_i	Constants for polynomial fit of $F(\overline{T})$	
b_i	Constants for polynomial fit of $F(\overline{T})$	

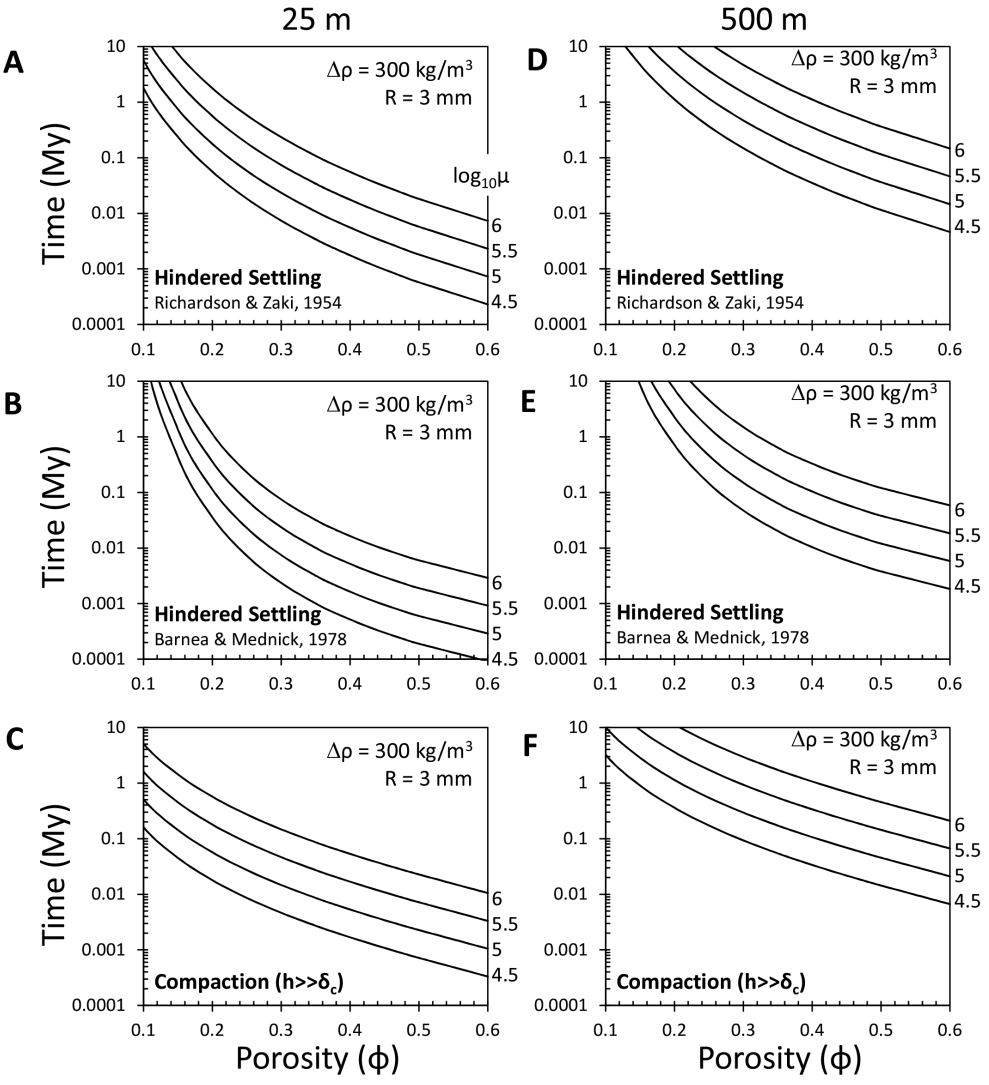

FIGURE 8. Time to generate a 25 m thick silicic boundary layer by hindered settling (**a** and **b**) and compaction (**c**). Figures **a** and **b** correspond to two different treatments of hindered settling. (**d**–**f**) These are the same as **a**–**c** except they represent the time to generate a 500 m thick boundary layer. Horizontal axis in all plots represents porosity, which is approximately equal to the melt fraction. Crystal radius of 3 mm and density contrast of 300 kg/m^3 are assumed. Curves in each plot correspond to different viscosities ($\log_{10}\mu$ in Pa s).

$$V = v\frac{\left(1-\chi\right)^2}{\left(1+\chi^{1/3}\right)^{5\chi/3(1-\chi)}} \quad (3)$$

where the symbols are the same as defined above. In both Equations 1 and 3, when the crystal fraction χ approaches one (or porosity $\phi = 1 - \chi$ approaches zero), settling velocities approach zero. Thus, even though hindered settling also scales with particle radius (see Eq. 2), the differential velocities are slow enough that separation of particles by size will be small. Figure 8 shows some estimates of the timescales for generating silica-rich boundary layers of a given thickness. Taking viscosities for wet (6–7 wt% H_2O) high silica *liquids* as 10^5 Pa s based on the results of the above rhyolite MELTS calculations and empirical formulations for viscosity (Hui and Zhang 2007) and density contrasts between solids and residual liquids during the last stages of crystallization of 300 kg/m^3, it can be seen that at porosities between 0.2–0.5 and a grain size of ~3 mm, it would take ~10 ky to expel 25 m of Si-rich granitic melt and ~10–100 ky to expel 500 m of melt. Because settling velocity scales inversely with viscosity of the liquid, increasing the viscosity to 10^6 to reflect less hydrous magmas would increase timescales of expulsion to 0.1–1 My.

Given that crystal grains are likely to form a penetrative, but porous framework at porosities lower than ~0.5–0.7 (Mooney 1951; Saar et al. 2001; Scott and Kohlstedt 2006), compaction may be a better description of melt segregation than hindered settling. We consider the case in which a porous crystal-rich mush (the magma chamber) rests on top of an impermeable boundary at its base. The mush compacts under its own weight, with the basal portions compacting first (decreasing porosity), driving expulsion of the interstitial melt through the top of the magmatic mush. The flow of melt relative to the compacting crystal matrix

can be described by Darcy flow, wherein the pressure gradient is driven by the buoyancy difference between crystals and melt. Melt velocity is zero at the base but increases upward, reaching a constant upward velocity if the scale height of the magma body is significantly larger than the compaction length scale, which is the length scale over which the crystal framework compacts. The compaction length scale δ_c is given by

$$\delta_c = \left[\frac{\varsigma + 4\eta/3}{\mu} k_\phi\right]^{1/2} \quad (4)$$

where ζ and η are the effective bulk and shear viscosities of the matrix, μ is the viscosity of the melt, and k_ϕ is the permeability, all of which depend on porosity ϕ (McKenzie 1984, 1987). For spherical grains, permeability can be approximated as (Bear 1972; Carman 1937; Kozeny 1927)

$$k_\phi = \frac{R^2\phi^3}{180(1-\phi)^2} \quad (5)$$

For porosities between 0.2–0.6 and grain radii of ~3 mm, k_ϕ is on the order of 10^{-8} to 10^{-9} m^2. Effective bulk and shear viscosities of the matrix are difficult to determine, but for porosities >0.3, might be on the order of 10^{13} to 10^{15} Pa s (Bachmann and Bergantz 2004; Jackson et al. 2003; Rabinowicz et al. 2001). Using a representative melt viscosity of ~10^5 Pa s for a hydrous Si-rich melt (Fig. 7f) yields compaction length scales <1 m for magmatic mushes (using higher melt viscosities would further decrease the compaction length scale). Given that the scale height of the magma chamber is on length scales of kilometers and, hence, much greater than any compaction length scale, the relative velocity w_o between the melt and crystal framework at the top of the magma body can be approximated by Darcy flow

$$w_o = \frac{k_\phi(1-\phi)\Delta\rho g}{\mu\phi} \quad (6)$$

The actual rate at which a crystal-free melt layer thickens at the top of magma body is $w_o\phi$. For porosities between 0.2–0.4, we find that a 25 m thick layer requires 1–10 ky to form and a 500 m thick layer requires ~100 ky (Fig. 8). In all cases, if we adopt a viscosity of 10^6 Pa s, timescales for extraction increase 10-fold. We note that our simplified approach in estimating the thickness of the extracted melt layer by compaction assumes that the height of the magma chamber is much larger than the compaction length scale. Our approach differs from that of Bachmann and Bergantz (2004). They estimated the characteristic time over which the melt in the magma chamber is drained by e-fold (e.g., by ~1/2.7). This not only requires assuming a magma chamber size, which is not known, but also assumes that silicic boundary layers are formed only after e-fold drainage of the melt. Recent work shows that most plutons do not efficiently drain (Lee and Morton 2015).

Magma chamber lifespan and the role of water and latent heat

Can a magma body remain partially molten long enough for compaction/hindered settling to occur? The lifespan of a magma body depends on the efficiency of heat loss and gain. Heat loss rates depend on the nature of heat transfer (magma convection, conduction, or hydrothermal circulation in the country rock) and the thermal state of the country rock. Heat gain occurs by magmatic recharge and release of latent heat (Gelman et al. 2013; Marsh 1981). Release of latent heat applies to all crystallizing magma bodies, but how latent heat is released during the crystallization interval (from liquidus to solidus) may play an important role in the formation and segregation of silica-rich melts. To illustrate, we first consider the general case of constant latent heat release over the crystallization interval (e.g., constant melt productivity) for a non-convecting magma body. In this case, the thermal evolution of the magma body can be modeled by heat diffusion

$$\rho_m c\frac{\partial T}{\partial t} + \rho_m L\frac{\partial F}{\partial T}\frac{\partial T}{\partial t} = -k\nabla^2 T \quad (7)$$

where ρ is density (kg/m^3), c is the specific heat (J/kg/°C), T is temperature (°C), t is time, k is thermal conductivity (Wm/°C), F is the liquid fraction (which varies from 0 at the solidus temperature to 1 at the liquidus temperature), and $\partial F/\partial T$ is the melt productivity per unit increase in T. L is the *total* latent heat released (J/kg) between the liquidus and solidus temperatures. If $\partial F/\partial T$ is constant over a particular temperature interval, then non-dimensionalizing Equation 7 results in the following expression for the characteristic diffusion time for a cooling magma body

$$t \sim \frac{x^2}{\kappa}\left(1 + \frac{L}{c}\frac{\partial F}{\partial T}\right) \quad (8)$$

where x is the characteristic size (e.g., radius) of the magma body and κ is the thermal diffusivity [$k/(\rho c)$]. If $L = 0$, Equation 8 simplifies to the conventional thermal diffusion timescale $t \sim x^2/\kappa$. For typical values of total L (40 kJ/kg) (Lange et al. 1994), c (1000 J/kg/°C), and κ (10^{-6} m^2/s) and assuming a 300 °C melting interval over which $F(T)$ is perfectly linear, the second term in parentheses is ~1.3, which means that the release of latent heat increases the lifespan of a magma body by a factor of ~2.

The problem becomes more interesting when we consider $F(T)$ to be nonlinear as shown above. Based on the rhyolite MELTS model outputs (Figs. 7a and 7b), we parameterize F with a sixth-order polynomial (Appendix Table 7[1])

$$F = \sum_{i=1}^{6} a_i \overline{T}^i \quad (9)$$

where temperature is normalized to the difference between the liquidus temperature T_L and solidus temperature T_S:

$$\overline{T} = \frac{T - T_S}{T_L - T_S} \quad (10)$$

T_S, T_L, and the curvature of $F(T)$, as expressed in terms of the polynomial coefficients a_i, depend on bulk composition and pressure (for the purposes of this study, we assume one bulk composition and pressure of 3 kbar). To predict melt compositions, we also parameterized our rhyolite MELTS-modeled SiO_2 concentrations of the melt (on an anhydrous basis) as a function of temperature with a sixth-order polynomial (Appendix Table 7[1])

$$SiO_2(\text{melt}) = \sum_{i=0}^{6} b_i \overline{T}^i \quad (11)$$

In water-bearing systems, progressive crystallization causes the residual liquid's dissolved water content to increase, eventually leading to saturation in a free fluid (water) phase. When

a free fluid phase appears, the thermodynamic variance of the system decreases, causing the system to behave like a eutectic (Vielzeuf and Schmidt 2001) so that melt productivity is highest just above the solidus. Under dry conditions, the eutectoid behavior is reduced, which is manifested as near constant melt productivity (dF/dT) or linear F over the melting interval. By contrast, the nonlinearity in $F(T)$ in water-bearing systems delays the release of latent heat and hence the bulk of the crystallization to late in a magma body's thermal life. For example, for a bulk water content of 6 wt%, 80% of the crystallization and release of latent heat is delayed to temperatures within 20% of the solidus ($\overline{T} < 0.2$) (Fig. 7b), consistent with experimental results (Marsh 1981; Pamukcu et al. 2013; Scaillet et al. 1997). By contrast, for relatively dry systems (0.3 wt% H_2O), 90% of the magma crystallizes at temperatures well above the solidus ($\overline{T} > 0.2$) (Fig. 7b). The extent to which crystallization is delayed correlates with bulk water content because higher bulk water contents cause fluid saturation to occur at higher normalized temperatures and higher melt fractions, F.

To apply these concepts, we solved Equation 7 for a variable dF/dT by forward finite difference using the following formula to calculate temperature at time step j

$$T_{i,j+1} = \left(\frac{-\kappa}{1+(dF/dT)L/c}\right)\left[\frac{T_{i+1,j} - 2T_{i,j} + T_{i-1,j}}{\Delta x^2}\right]\Delta t + T_{i,j} \quad (11)$$

where i is the spatial index, Δt is the time increment, and Δx is the spatial increment. Initial temperature of the magma body was taken to be the liquidus temperature, which varies with water content. We adopted a total latent heat L of 40 kJ/kg (Lange et al. 1994) and assumed this value to be constant regardless of water content, which we confirmed using the MELTS model outputs. The initial wall rock temperature was set at 400 °C. A typical thermal diffusivity of 10^{-6} m/s^2 was assumed. We assumed that the magma body was tabular in shape and that the smallest dimension is its thickness. Although we do not know the thickness of the magma body, we assume a value of 5 km to approximate a pluton that extends throughout the upper crust [based on Al-in-hornblende barometry from Ague and Brimhall (1988b)]. Temperature dependency on thermal diffusivity would increase magma lifespan slightly (Gelman et al. 2013; Whittington et al.

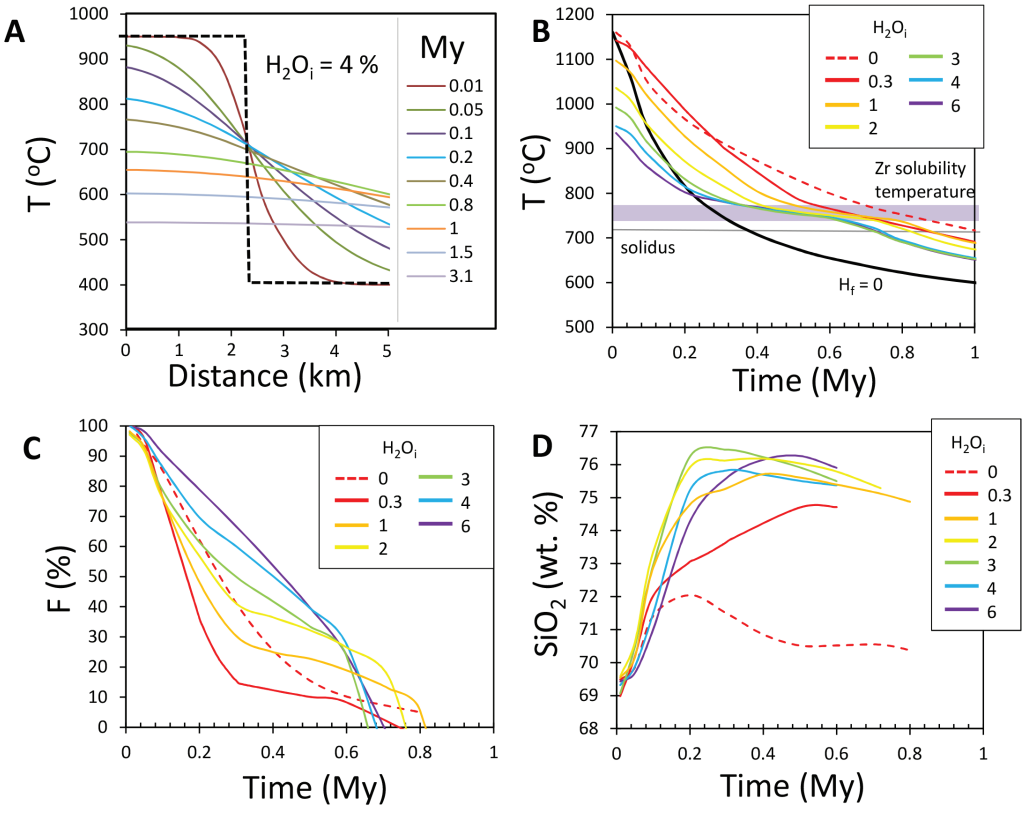

Figure 9. (**a**) Thermal evolution of a 5 km thick tabular magma body intruded into a country rock with a background temperature of 400 °C. Initial temperature of the magma is assumed to correspond to its liquidus, which we assume here to correspond to a tonalitic liquid with 4 wt% H_2O. Temperature profiles for different times are shown. Thermal model assumes thermal conduction with the effect of latent heat, but convection is ignored. Dashed line represents initial condition. (**b**) Temperature of the center of the magma body as a function of time for systems with different bulk water contents (closed system is assumed). Initial temperature of the magma corresponds to liquidus temperature at relevant water content. Each colored line represents a model for different bulk water contents. All models assume a constant total latent heat, but different functional forms of $F(\overline{T})$. Black curved line corresponds to the unrealistic scenario where total latent heat is zero. (**c**) Melt fraction at the center of the cooling magma body as a function of time. (**d**) SiO_2 content of the residual liquid as a function of time. SiO_2 contents for melt fractions less than ~15% are not reported. (Color online.)

2009), but was ignored here to isolate the effect of latent heat. In addition to ignoring magma convection, we have also ignored hydrothermal circulation, both of which would hasten the cooling of the magma body.

Our thermal models are shown in Figure 9. The lifespan (time above solidus) of a single-stage magma body emplaced into the upper crust and conductively cooled without latent heat ($L = 0$) is ~0.4 My (Fig. 9b). This is just long enough for a liquid boundary layer of 25 m to segregate by compaction. When latent heat is considered, regardless of the amount of system water content, the characteristic cooling times of tonalitic magmas are 0.8 My, as predicted from simple scaling (Eq. 8). This increase in cooling time allows for a much thicker boundary layer to form. However, the most interesting effect is that water modulates the amount of time the magma body spends at near solidus conditions and the amount of water-rich, high-silica melts that can be generated (Fig. 9c). Wet magmas that reach water saturation early will delay most of the crystallization to near solidus temperatures, causing prolonged thermal arrest at the temperatures and melt fractions in which high silica residual liquids are generated. As can be seen in Figure 9d, wet magmas generate more silica-rich melts during their lifespans while the delayed release of latent heat in water-bearing systems, prolongs the relative time interval over which silicic liquids can be expelled.

What is the importance of water in generating granites?

Our observations on the generation and extraction of silicic magmas may have more general implications for making silicic melts, such as granite. Numerous studies have argued that granite formation requires water and that because Earth has water, it has granites and continents (Campbell and Taylor 1983; Rosing et al. 2006; Watson and Harrison 2005). For instance, although granites can be found in relatively dry magmatic systems, such as at spreading ridges and hotspots on Earth (Carmichael 1964) and even on the Moon (Bonin 2012; Warren et al. 1983), the volume of such granites is negligible compared to the volumes of granites found in subduction zones where water is available from the parental basalts. There is no debate that the formation of large volumes of granite requires water, but there are several reasons why water is important.

The standard view is that because water reduces the melting point of rocks and makes it easier to heat rocks to their melting points (Patino Douce and Johnston 1991; Vielzeuf and Schmidt 2001), hence granites mostly form by up-temperature processes, that is, by partial melting of pre-existing crust (crustal anatexis) rather than by down-temperature crystallization from a hot, more primitive magma. Low zircon crystallization temperatures (700 °C) inferred from Ti contents of zircon have occasionally been argued to indicate an origin by water-saturated partial melting (Watson and Harrison 2005). However, metasediments or metabasalts do not typically have enough bound water to always melt under water-saturated conditions (Rutter and Wyllie 1988). Melting the crust requires heat, which commonly comes from intrusion or underplating of hot magmas like basalts for crustal and upper mantle thermal states typical of most of Earth's history (Dufek and Bergantz 2005; Jackson et al. 2003; Rutter and Wyllie 1988), but it has been shown that such heating is inefficient in producing significant amounts of anatexis (Dufek and Bergantz 2005). There is, of course, no doubt that some types of granitoids form by melting of metasediments (Chappell 1999; Chappell et al. 1992), but whether the majority granites form by anatexis is debated.

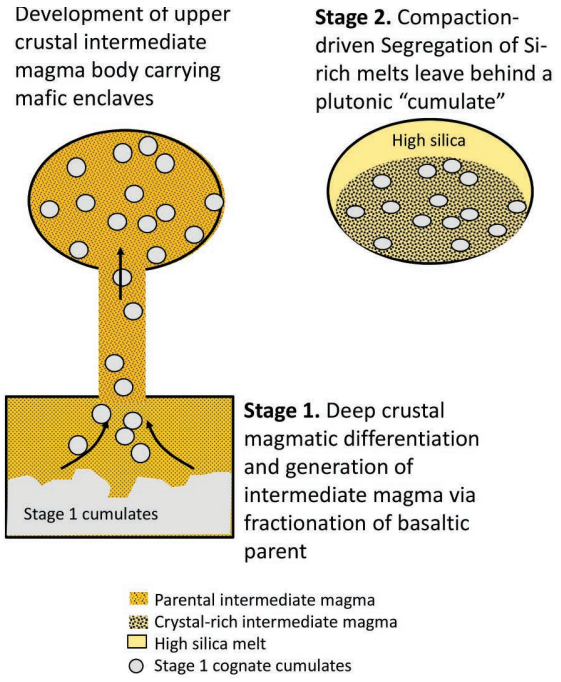

Figure 10. Hypothetical model for the formation of granites by crystal-liquid segregation. Stage 1. An intermediate magma (60–70 wt% SiO_2) is generated in a deep crustal magma chamber by crystal fractionation of a more primitive and mafic parent. The intermediate magma is evacuated from the deep crustal magma chamber, entraining some of its own cumulates (mafic enclaves). This intermediate magma along with its cumulate cargo is emplaced in the shallow crust. In Stage 2, the magma body cools isobarically. Residual liquids rich in water and silica form with progressive crystallization. Residual liquids are expelled to the sides and roof of the magma body by compaction and/or hindered settling, generating a crystal-poor silicic boundary layer. The crystal-rich mush represents a restite/cumulate of the silicic melt in the boundary layer. (Color online.)

Here, we argue that any moderately hydrous (>2 wt%) parental magma will reach water saturation and minimum melting temperatures by crystal fractionation during cooling or decompression during ascent (Albarede 1983; Cann 1970). Thus, the ubiquity of granites can be explained if granites dominantly form by down-temperature crystal fractionation of hydrous magmas. This view is similar to that in other studies based on indirect constraints from ignimbrite stratigraphy or from magma Zr concentrations that suggest higher temperatures than that inferred from Ti in zircon thermometry (Gelman et al. 2013; Hildreth 1979; Hildreth and Wilson 2007; Lee and Bachmann 2014; Miller et al. 2003; Wade et al. 2005). Most trace-element or isotopic signatures indicative of crustal assimilation are likely inherited from more mafic and hence parental magmas that assimilated crust in deep crustal magmatic zones, where background temperatures are high, making it easier to assimilate the wallrock (Annen et al. 2006; Hildreth and Moorbath 1988).

Implications: Prospects and limitations of making high silica magmas by crystal fractionation

We show from a unique outcrop that silicic melts can form by compaction driven segregation from a partially crystallized intermediate magma, confirming other studies based on geochemical systematics (Bachmann and Bergantz 2004, 2008; Lee and Bachmann 2014; Putirka et al. 2007). We suggest that granites can be readily formed by crystal-fractionation from intermediate magmas undergoing compaction or hindered settling, though we cannot draw from our study whether such processes are dominant. Nevertheless, we envision the following scenario for the formation of granites (Fig. 10). Mantle-derived hydrous basalts rise into the lower crust, where they stall and cool. Crystal fractionation generates deep crustal mafic cumulates and intermediate residual magmas (andesites to dacites) (Canil et al. 2010; DeBari and Sleep 1991; Ducea 2001, 2002; Greene et al. 2006; Hacker et al. 2008; Hildreth and Moorbath 1988; Jagoutz and Schmidt 2012; Jagoutz 2010; Lee et al. 2006, 2012, 2007). These intermediate magmas then ascend into the upper crust, carrying a cargo of mafic enclaves (Barbarin 2005; Barbarin et al. 1989; Farner et al. 2014; Paterson et al. 1989). These intermediate magmas continue to cool and crystallize, which causes residual melts to become more water- and silica-rich. The Si-rich melts are expelled from the intermediate magma mush, generating Si-rich boundary layers at the tops of the magma bodies. The remaining magmatic mush crystallizes into a pluton, which, by definition, is the adcumulate (crystals + interstitial trapped liquid) complement to the high silica melt [conceptually, this adcumulate/restite is similar to that described in (Langmuir 1989)]. Because of the small amounts of melts formed, the composition of this cumulate pluton should be nearly indistinguishable from that of an intermediate parental magma itself, especially if there is trapped melt (Lee and Morton 2015). This may explain why granitoid plutonic rocks appear to have compositions that can be modeled as silicate liquids but at the same time have textures suggestive of a cumulate origin (Vernon 1986). There is some potential for using trace elements to help distinguish silicic cumulates from silicic melts (Deering and Bachmann 2010; Gelman et al. 2014; Lee and Morton 2015).

In summary, down-temperature crystal fractionation of more mafic, hotter parents to form granites is a viable process (Bowen 1915, 1928; Bucholz et al. 2014; Deering and Bachmann 2010; Jagoutz and Schmidt 2012; Jagoutz 2010; Lee and Bachmann 2014). Water significantly enhances the efficiency of making granites because it lowers melt viscosity, increases silica activity, and suppresses much of the crystallization to late in the thermal life of the magma where water and silica activity are greatest. The latter effect prolongs the lifespan of the magma at the time in which silicic melts are being produced, allowing more time for extraction from the crystal mush by hindered settling or compaction. However, simple mass balance shows that the total amount of granite that can be generated from a basaltic parental magma is ultimately small (<5% of original mass of basalt), consistent with the observation that only small volumes of granites are found in volcanic arcs (Lee and Morton 2015; Putirka et al. 2014).

Acknowledgments

We thank Tien Chang Lee, Helge Gonnermann, Olivier Bachmann, Monica Erdman, and Michael Manga for discussions. Guilherme Gualda, Jonathan Miller and Calvin Miller are thanked for insightful reviews. This work was supported by NSF OCE-1338842.

References cited

Ague, J.J., and Brimhall, G.H. (1988a) Magmatic arc asymmetry and distribution of anomalous plutonic belts in the batholiths of California: Effects of assimilation, crustal thickness and depth of crystallization. Geological Society of America Bulletin, 100, 912–927.

——— (1988b) Regional variations in bulk chemistry, mineralogy, and the compositions of mafic and accessory minerals in the batholiths of California. Geological Society of America Bulletin, 100, 891–911.

Albarede, F. (1983) Limitations thermiques a l'ascension des magmas hydrates. Comptes Rendus de l'Académie des Sciences, 296, 1441–1444.

Allen, C.M. (1992) A nested diapir model for the reversely zoned Turtle Pluton, southeastern California. Transactions of the Royal Society of Edinburgh, Earth Science, 83, 179–190.

Annen, C., Blundy, J.D., and Sparks, R.S.J. (2006) The genesis of intermediate and silicic magmas in deep crustal hot zones. Journal of Petrology, 47, 505–539.

Atherton, M.P. (1993) Granite magmatism. Journal of Geological Society of London, 150, 1009–1023.

Bachl, C.A., Miller, C.F., Miller, J.S., and Faulds, J.E. (2001) Construction of a pluton: evidence from an exposed cross-section of the Searchlight pluton, Ledorado Mountains, Nevada. Geological Society of America Bulletin, 113, 1213–1228.

Bachmann, O., and Bergantz, G.W. (2004) On the origin of crystal-poor rhyolites: extracted from batholithic crystal mushes. Journal of Petrology, 45, 1565–1582.

——— (2008) Rhyolites and their source mushes across tectonic settings. Journal of Petrology, 49, 2277–2285.

Bacon, C.R., and Druitt, T.H. (1988) Compositional evolution of the zoned calcalkaline magma chamber of Mount Mazama, Crater Lake, Oregon. Contributions to Mineralogy and Petrology, 98, 224–256.

Baker, B.H., and McBirney, A.R. (1985) Liquid fractionation. Part III: geochemistry of zoned magmas and the compositional effects of liquid fractionation. Journal of Volcanology and Geothermal Research, 24, 55–81.

Barbarin, B. (2005) Mafic magmatic enclaves and mafic rocks associated with some granitoids of the central Sierra Nevada batholith, California: Nature, origin, and relations with the hosts. Lithos, 80, 155–177.

Barbarin, B., Dodge, F.C.W., Kistler, R.W., and Bateman, P.C. (1989) Mafic inclusions, aggregates and dikes in granitoid rocks, central Sierra Nevada batholith, California—Analytic data. U.S.Geological Survey Bulletin, 1899, 28.

Barker, D.S. (2000) Emplacement of a xenolith-rich sill, Lajitas, Texas. Journal of Volcanology and Geothermal Research, 104, 153–168.

Barnea, E., and Mednick, R.L. (1978) A generalized approach to the fluid dynamics of particulate systems part III: General correlation for the pressure drop through fixed beds of spherical particles. The Chemical Engineering Journal, 15, 215–227.

Bear, J. (1972) Dynamics of Fluids in Porous Media. Elsevier, Amsterdam.

Beard, J.S., and Lofgren, G.E. (1991) Dehydration melting and water-saturated melting of basaltic and andesitic greenstones and amphibolites at 1, 3, and 6.9 kbar. Journal of Petrology, 32, 365–401.

Boehnke, P., Watson, E.B., Trail, D., Harrison, T.M., and Schmitt, A.K. (2013) Zircon saturation re-revisited. Chemical Geology, 351, 324–334.

Boettcher, A.L., and Wyllie, P.J. (1968) Melting of granite with excess water to 30 kilobars pressure. Journal of Geology, 76, 235–244.

Bonin, B. (2012) Extra-terrestrial igneous granites and related rocks: A review of their occurrence and petrogenesis. Lithos, 153, 3–24.

Bowen, N.L. (1915) The crystallization of haplodioritic, and related magmas. American Journal of Science, 40, 161–185.

——— (1928) The Evolution of the Igneous Rocks, 334 p. Princeton University Press, New Jersey.

Brown, M. (1994) The generation, segregation, ascent and emplacement of granitic magma: the migmatite-to-crustally derived granite connection in thickened orogenies. Earth Science Reviews, 36, 83–130.

Brown, M., Averkin, Y.A., and McLellan, E.L. (1995) Melt segregation in migmatites. Journal of Geophysical Research, 100, 15,655–15,679.

Bucholz, C.E., Jagoutz, O., Schmidt, M.W., and Sambuu, O. (2014) Fractional crystallization of high-K arc magmas: biotite- versus amphibole-dominated fractionation series in the Dariv Igneous complex, Western Mongolia. Contributions to Mineralogy and Petrology, 168, 1072.

Busby, C. (2004) Continental growth at convergent margins facing large ocean basins: a case study from Mesozoic convergent-margin basins of Baja California, Mexico. Tectonophysics, 392, 241–277.

Campbell, I.H., and Taylor, S.R. (1983) No water, no granites—No oceans, no continents. Geophysical Research Letters, 10, 1061–1064.

Canil, D., Styan, J., Larocque, J., Bonnet, E., and Kyba, J. (2010) Thickness and

composition of the Bonanza arc crustal section, Vancouver Island, Canada. Geological Society of America Bulletin, 122, 1094.
Cann, J.R. (1970) Upward movement of granitic magma. Geological Magazine, 107, 335–340.
Carman, P.C. (1937) Fluid flow through a granular bed. Transactions of the Institute of Chemical Engineering, London, 15, 150–156.
Carmichael, I.S.E. (1964) The petrology of Thingmuli, a tertiary volcano in Eastern Iceland. Journal of Petrology, 5, 435–460.
Castro, A. (2013) Tonalite-granodiorite suites as cotectic systems: a review of experimental studies with applications to granitoid petrogenesis. Earth-Science Reviews, 124, 68–95.
Castro, A., Gerya, T., García-Casco, A., Fernández, C., Déaz-Alvarado, J., Moreno-Ventas, I., and Löw, I. (2010) Melting relations of MORB-sediment mélanges in underplated mantle wedge plumes; implications for the origin of Cordilleran type batholiths. Journal of Petrology, 51, 1267–1295.
Chappell, B.W. (1999) Alumina saturation in I- and S-type granites and the characterization of fractionated haplogranites. Lithos, 49, 535–551.
Chappell, B.W., White, A.J.R., and Brown, P.E. (1992) I- and S-type granites in the Lachlan fold belt. Transactions of the Royal Society of Edinburgh, Earth Science, 83, 1–26.
Clemens, J.D., and Stevens, G. (2012) What controls chemical variation in granitic magmas? Lithos, 134-135, 317–329.
Coleman, D.S., Gray, W., and Glazner, A.F. (2004) Rethinking the emplacement and evolution of zoned plutons: geochronologic evidence for incremental assembly of the Tuolumne Intrusive Suite, California. Geology, 32, 433–436.
DeBari, S.M., and Sleep, N.H. (1991) High-Mg, low-Al bulk composition of the Talkeetna island arc, Alaska: implications for primary magmas and the nature of arc crust. Geological Society of America Bulletin, 103, 37–47.
Deering, C.D., and Bachmann, O. (2010) Trace element indicators of crystal accumulation in silicic igneous rocks. Earth and Planetary Science Letters, 297, 324–331.
Ducea, M. (2001) The California arc: thick granitic batholiths, eclogitic residues, lithosphere-scale thrusting, and magmatic flare-ups. Geological Society of America Today, 11, 4–10.
——— (2002) Constraints on the bulk composition and root foundering rates of continental arcs: A California arc perspective. Journal of Geophysical Research, 107, ECV 15-1–ECV 15-13, http://dx.doi.org/10.1029/2001JB000643.
Dufek, J., and Bachmann, O. (2010) Quantum magmatism: magmatic compositional gaps generated by melt-crystal dynamics. Geology, 38, 687–690.
Dufek, J., and Bergantz, G.W. (2005) Lower crustal magma genesis and preservation: a stochastic framework for the evaluation of basalt-crust interaction. Journal of Petrology, 46, 2167–2195.
Farner, M.J., Lee, C.-T.A., and Putirka, K.D. (2014) Mafic-felsic magma mixing limited by reactive processes: a case study of biotite-rich rinds on mafic enclaves. Earth and Planetary Science Letters, 393, 49–59.
Fridrich, C.J., and Mahood, G. (1984) Reverse zoning in the resurgent intrusions of the Grizzly Peak cauldron, Sawatch Range, Colorado. Geological Society of America Bulletin, 95, 779–787.
Gastil, R.G. (1975) Plutonic zones of the Peninsular Ranges of southern California and northern Baja California. Geology, 3, 361–363.
Gastil, G., Morgan, G., and Krummenacher, D. (1988) The tectonic history of Peninsular California and adjacent Mexico. In W.G. Ernst, Ed., Metamorphic and Tectonic Evolution of the Penisular Ranges Batholith. Metamorphism and crustal evolution of the western United States, Rubey Volume VII, p. 286–306. Prentice-Hall, Englewood Cliffs, New Jersey.
Gelman, S.E., Gutierrez, F.J., and Bachmann, O. (2013) On the longevity of large upper crustal silicic magma reservoirs. Geology, 41, 759–762.
Gelman, S.E., Deering, C.D., Bachmann, O., Huber, C., and Guiterrez, F.J. (2014) Identifying the crystal graveyards remaining after large silicic eruptions. Earth and Planetary Science Letters, 403, 299–306.
Glazner, A.F., Coleman, D.R., and Bartley, J.M. (2008) The tenuous connection between high-silica rhyolites and granodiorite plutons. Geology, 36, 183–186.
Greene, A.R., DeBari, S.M., Kelemen, P.B., Blusztajn, J., and Clift, P.D. (2006) A detailed geochemical study of island arc crust: The Talkeetna arc section south-central Alaska. Journal of Petrology, 47, 1051–1093.
Gualda, G.A.R., Ghiorso, M.S., Lemons, R.V., and Carley, T.L. (2012) rhyolite-MELTS: a modified calibration of MELTS optimized for silica-rich, fluid-bearing magmatic systems. Journal of Petrology, 53, 875–890.
Hacker, B., Mehl, L., Kelemen, P., Rioux, M., Behn, M., and Luffi, P. (2008) Reconstruction of the Talkeetna intraoceanic arc of Alaska through thermobarometry. Journal of Geophysical Research, 113, B03204.
Hildreth, W. (1979) The Bishop Tuff: Evidence for the origin of compositional zonation in silicic magma chambers. Geological Society of American Special Paper, 180, 43–75.
Hildreth, W., and Moorbath, S. (1988) Crustal contributions to arc magmatism in the Andes of central Chile. Contributions to Mineralogy and Petrology, 98, 455–489.
Hildreth, W., and Wilson, C.J.N. (2007) Compositional zoning of the Bishop Tuff. Journal of Petrology, 48, 951–999.
Holloway, J.R., and Burnham, C.W. (1972) Melting relations of basalt with equilibrium water pressure less than total pressure. Journal of Petrology, 13, 1–29.
Huang, W.-L., and Wyllie, P.J. (1986) Phase relationships of gabbro-tonalite-granite-water at 15 kbar with applications to differentiatoin and anatexis. American Mineralogist, 71, 301–316.
Hui, H., and Zhang, Y. (2007) Toward a general viscosity equation for natural anhydrous and hydrous silicate melts. Geochimica et Cosmochimica Acta, 71, 403–416.
Hutchinson, R.M. (1956) Structure and petrology of Enchanted Rock Batholith, Llano and Gillespie counties, Texas. Geological Society of America Bulletin, 67, 763–806.
Jackson, M.D., Cheadle, M.J., and Atherton, M.P. (2003) Quantitative modeling of granitic melt generation and segregation in the continental crust. Journal of Geophysical Research, 108, 2332, http://dx.doi.org/10.1029/2001JB001050.
Jagoutz, O.E. (2010) Construction of the granitoid crust of an island arc. Part II: A quantitative petrogenetic model. Contributions to Mineralogy and Petrology, 160, 359–381.
Jagoutz, O., and Schmidt, M.W. (2012) The formation and bulk composition of modern juvenile continental crust: The Kohistan arc. Chemical Geology, 298-299, 79–96.
Jahns, R.H., and Burnham, C.W. (1969) Experimental studies of pegmatite genesis: I. A model for the derivation and crystallization of granitic pegmatites. Economic Geology, 64, 843–864.
Kawamoto, T. (1996) Experimental constraints on differentiation and H_2O abundance of calc-alkaline magmas. Earth and Planetary Science Letters, 144, 577–589.
Kistler, R.W., Wooden, J.L., and Morton, D.M. (2003) Isotopes and ages in the northern Peninsular Ranges batholith, southern California. U.S. Geological Survey Open-File Report, 03-489, 45.
Kozeny, J. (1927) Uber kapillare leitung des wassers im boden. Sitzungsber, Akademie der Wissenschaften(136).
Lange, R.A., Cashman, K.V., and Navrotsky, A. (1994) Direct measurements of latent heat during crystallization and melting of a ugandite and an olivine basalt. Contributions to Mineralogy and Petrology, 118, 169–181.
Langmuir, C.H. (1989) Geochemical consequences of in situ crystallization. Nature, 340, 199–205.
Lee, C.-T.A., and Bachmann, O. (2014) How important is the role of crystal fractionation in making intermediate magmas? Insights from Zr and P systematics. Earth and Planetary Science Letters, 393, 266–274.
Lee, C.-T.A., and Morton, D.M. (2015) High silica granites: terminal porosity and crystal settling. Earth and Planetary Science Letters, 409, 23–31.
Lee, C.-T.A., Cheng, X., and Horodyskyj, U. (2006) The development and refinement of continental arcs by primary basaltic magmatism, garnet pyroxenite accumulation, basaltic recharge and delamination: insights from the Sierra Nevada, California. Contributions to Mineralogy and Petrology, 151, 222–242.
Lee, C.-T.A., Morton, D.M., Kistler, R.W., and Baird, A.K. (2007) Petrology and tectonics of Phanerozoic continent formation: from island arcs to accretion and continental arc magmatism. Earth and Planetary Science Letters, 263, 370–387.
Lee, C.-T.A., Oka, M., Luffi, P., and Agranier, A. (2009) Internal distribution of Li and B in serpentinites from the Feather River Ophiolite, California based on laser ablation inductively coupled plasma mass spectrometry. Geochemistry, Geophysics, Geosystems, 9, Q12011, http://dx.doi.org/10.1029/2008GC002078.
Lee, C.-T.A., Luffi, P., Chin, E.J., Bouchet, R., Dasgupta, R., Morton, D.M., Le Roux, V., Yin, Q.-Z., and Jin, D. (2012) Copper systematics in arc magmas and implications for crust-mantle differentiation. Science, 336, 64–68.
Lee, C.-T.A., Lee, T.-C., and Wu, C.-T. (2014) Modeling the compositional evolution of recharging, evacuating, and fractionating (REFC) magma chambers: Implications for differentiation of arc magmas. Geochimica et Cosmochimica Acta, 143, 8–22.
Leighton, D., and Acrivos, A. (1987) measurement of shear-induced self-diffusion in concentrated suspensions of spheres. Journal of Fluid Mechanics, 177, 109–131.
Lejeune, A.M., and Richet, P. (1995) Rheology of crystal-bearing silicate melts: an experimental study at high viscosities. Journal of Geophysical Research, 100, 4215–4229.
Liao, K., Morton, D.M., and Lee, C.-T.A. (2013) Geochemical diagnostics of metasedimentary dark enclaves: a case study from the Peninsular Ranges Batholith, southern California. International Geology Review, 55, 1049–1072.
Lipman, P.W. (2007) Incremental assembly and prolonged consolidatio nof Cordilleran magma chambers: evidence from the southern Rocky Mountain volcanic field. Geosphere, 3, 42.
Lundstrom, C. (2009) Hypothesis for the origin of convergent margin granitoids and Earth's continental crust by thermal migration zone refining. Geochimica et Cosmochimica Acta, 73, 5709–5729.
Mader, H.M., Llewellin, E.W., and Mueller, S.P. (2013) The rheology of two phase magmas: a review and analysis. Journal of Volcanology and Geothermal Research, 257, 135–158.
Marsh, B.D. (1981) On the crystallinity, probability of occurrence, and rheology

of lava and magma. Contributions to Mineralogy and Petrology, 78, 85–98.
McBirney, A.R. (1980) Mixing and unmixing of magmas. Journal of Volcanology and Geothermal Research, 7, 357–371.
——— (1995) Mechanisms of differentiation in the Skaergaard intrusion. Journal of the Geological Society London, 152, 421–435.
McKenzie, D. (1984) The generation and compaction of partially molten rock. Journal of Petrology, 25, 713–765.
——— (1987) The compaction of igneous and sedimentary rocks. Journal of the Geological Society London, 144, 299–307.
Miller, C.F., McDowell, S.M., and Mapes, R.W. (2003) Hot and cold granites? Implications of zircon saturation temperatures and preservation of inheritance. Geology, 31, 529–532.
Moitra, P., and Gonnermann, H.M. (2015) Effects of crystal shape- and size-modality on magma rheology. Geochemistry, Geophysics, Geosystems, 16, 1–26, http://dx.doi.org/10.1002/2014GC005554.
Mooney, M. (1951) The viscosity of a concentrated suspension of spherical particles. Journal of Colloid Science, 6, 162–170.
Morton, D.M., Miller, F.K., Kistler, R.W., Premo, W.R., Lee, C.-T.A., Langenheim, V.E., Wooden, J.L., Snee, L.W., Clausen, B.L., and Cossette, P. (2014) Framework and petrogenesis of the northern Peninsular Ranges batholith, southern California. Geological Society of American Memoirs, 211, 61–143.
Noyes, H.J., Wones, D.R., and Frey, F.A. (1983) A tale of two plutons: petrographic and mineralogic constraints on the petrogenesis of the Red Lake and Eagle Peak plutons, central Sierra Nevada, California. Journal of Geology, 91, 353–379.
Pamukcu, A.S., Carley, T.L., Gulada, G.A.R., Miller, C.F., and Ferguson, C.A. (2013) The evolution of the Peach Spring giant magma body: Evidence from accessory mineral textures and compositions, bulk pumice and glass geochemistry, and rhyolite-MELTS modeling. Journal of Petrology, 54, 1109–1148.
Paterson, S.R., Vernon, R.H., and Tobisch, O.T. (1989) A review of criteria for the identification of magmatic and tectonic foliations in granitoids. Journal of Structural Geology, 11, 349–363.
Patino Douce, A.E., and Johnston, A.D. (1991) Phase equilibria and melt productivity in the pelitic system: implications for the origin of peraluminous granitoids and aluminous granulites. Contributions to Mineralogy and Petrology, 107, 202–218.
Philpotts, A.R. (1976) Silicate liquid immiscibility: its probable extent and petrogenetic significance. American Journal of Science, 276, 1147–1177.
Pitcher, W.S. (1997) The Nature and Origin of Granite. Chapman and Hall, London.
Plank, T., Kelley, K.A., Zimmer, M.M., Hauri, E.H., and Wallace, P.J. (2013) Why do mafic arc magmas contain ~4 wt% water on average? Earth and Planetary Science Letters, 364, 168–179.
Putirka, K.D., Perfit, M., Ryerson, F.J., and Jackson, M.G. (2007) Ambient and excess mantle temperatures, olivine thermometry, and active vs. passive upwelling. Chemical Geology, 241, 177–206.
Putirka, K.D., Canchola, J., Rash, J., Smith, O., Torrez, G., Paterson, S.R., and Ducea, M.N. (2014) Pluton assembly and the genesis of granitic magmas: insights from the GIC pluton in cross section. Sierra Nevada Batholith, California. American Mineralogist, 99, 1284–1303.
Rabinowicz, M., Genthon, P., Ceuleneer, G., and Hillairet, M. (2001) Compaction in a mantle mush with high melt concentrations and the generation of magma chambers. Earth and Planetary Science Letters, 188, 313–328.
Ratajeski, K., Sisson, T.W., and Glazner, A.F. (2005) Experimental and geochemical evidence for derivation of the El Capitan Granite, California, by partial melting of hydrous gabbroic lower crust. Contributions to Mineralogy and Petrology, 149, 713–734.
Richardson, J.F., and Zaki, W.N. (1954) The sedimentation of a suspension of uniform spheres under conditions of viscous flow. Chemical Engineering Science, 3, 65–73.
Roedder, E. (1951) Low-temperature liquid immiscibility in the system K_2O-FeO-Al_2O_3-SiO_2. American Mineralogist, 84, 1346–1353.
Rosing, M.T., Bird, D.K., Sleep, N.H., Glassley, W., and Albarede, F. (2006) The rise of continents—an essay on the geologic consequences of photosynthesis. Palaeogeography, Palaeoclimatology, Palaeoecology, 232, 99–113.
Ross, M.E. (1986) Flow differentiation, phenocryst alignment, and compositional trends within a dolerite dike at Rockport, Massachusetts. Geological Society of America Bulletin, 97, 232–240.
Rutter, M.J., and Wyllie, P.J. (1988) Melting of vapour-absent tonalite at 10 kbar to simulate dehydration-melting in the deep crust. Nature, 331, 159–160.
Saar, M.O., Manga, M., Cashman, K.V., and Fremouw, S. (2001) Numerical models of the onset of yield strength in crystal-melt suspensions. Earth and Planetary Science Letters, 187, 367–379.
Scaillet, B., Holtz, F., and Pichavant, M. (1997) Rheological properties of granitic magmas in their crystallization range. In J.L. Bouchez, D.H.W. Hutton, and W.E. Stephens, Eds. Granite: From segregation of melt to emplacement fabrics, p. 11–29. Kluwer, Dordrecht, Netherlands.
Scott, T., and Kohlstedt, D.L. (2006) The effect of large melt fraction on deformation behavior of peridotite. Earth and Planetary Science Letters, 246, 177–187.
Snabre, P., and Pouligny, B. (2008) Size segregation in a fluid-like or gel-like suspension settling under gravity or in a centrifuge. Langmuir, 24, 13,338–13,347.
Taylor, S.R., and McLennan, S.M. (1985) The Continental Crust: Its composition and evolution. Blackwell, Oxford.
Todd, V.R., Erskine, B.G., and Morton, D.M. (1988) Metamorphic and tectonic evolution of the Penisular Ranges batholith. In W.G. Ernst, Ed., Metamorphism and Crustal Evolution of the Western United States, Rubey Volume VII, p. 894–937. Prentice-Hall, Englewood Cliffs, New Jersey.
Turi, B., and Taylor, H.P. Jr. (1971) An oxygen and hydrogen isotope study of a granodiorite pluton from the southern California batholith. Geochimica et Cosmochimica Acta, 35, 383–406.
Tuttle, O.F., and Bowen, N.L. (1958) Origin of granite in the light of experimental studies in the system $NaAlSi_3O_8$-$KAlSi_3O_8$-SiO_2-H_2O. Geological Society of American Memoirs, 74, 1–146.
Van Tongeren, J.A., and Mathez, E.A. (2012) Large-scale liquid immiscibility at the top of the Bushveld Complex. Geology, 40, 491–494.
Vernon, R.H. (1986) K-feldspar megacrysts in granites—Phenocrysts, not porphyroblasts. Earth-Science Reviews, 23, 1–63.
Vielzeuf, D., and Schmidt, M.W. (2001) Melting relations in hydrous systems revisited: application to metapelites, metagreywackes and metabasalts. Contributions to Mineralogy and Petrology, 141, 251–267.
Wade, J.A., Plank, T., Stern, R.J., Tollstrup, D.L., Gill, J.B., O'Leary, J.C., Eiler, J.M., Moore, R.B., Woodhead, J.D., Trusdell, F., Fischer, T.P., and Hilton, D.R. (2005) The may 2003 eruption of Anatahan volcano, Mariana Islands: geochemical evolution of a silicic island-arc volcano. Journal of Volcanology and Geothermal Research, 146, 139–170.
Wark, D.A., and Watson, E.B. (2006) TitaniQ: a titanium-in-quartz geothermometer. Contributions to Mineralogy and Petrology, 152, 743–754.
Warren, P.H., Taylor, G.J., Keil, K., Shirley, D.N., and Wasson, J.T. (1983) Petrology and chemistry of two "large" granite clasts from the moon. Earth and Planetary Science Letters, 64, 175–185.
Watson, E.B., and Harrison, T.M. (1983) Zircon saturation revisited: temperature and composition effects in a variety of crustal magma types. Earth and Planetary Science Letters, 64, 295–304.
——— (2005) Zircon thermometer reveals minimum melting conditions on earliest Earth. Science, 841–844.
Whittington, A.G., Hofmeister, A.M., and Nabelek, P.I. (2009) Temperature-dependent thermal diffusivity of Earth's crust and implications for magmatism. Nature, 458, 319–321.

Manuscript received July 10, 2014
Manuscript accepted May 3, 2015
Manuscript handled by Calvin Miller